JACS
JOURNAL OF THE AMERICAN CHEMICAL SOCIETY

Article

pubs.acs.org/JACS

Architecture of Chiral Poly(phenylacetylene)s: From Compressed/Highly Dynamic to Stretched/Quasi-Static Helices

Rafael Rodríguez, Emilio Quiñoá, Ricardo Riguera,* and Félix Freire*

Centro Singular de Investigación en Química Biolóxica e Materiais Moleculares (CIQUS) and Departamento de Química Orgánica Universidade de Santiago de Compostela, 15782 Santiago de Compostela, Spain

Supporting Information

ABSTRACT: The remarkable consequences in elongation, dynamic character, response to external stimuli (e.g., solvent effects, metal cations), and aggregation observed in helical poly(phenylacetylene)s (PPAs) when either the type of linkage with the pendant groups (i.e., anilide, benzamide) or the aromatic substitution pattern (i.e., *ortho*, *meta*, *para*) of the parent phenylacetylene monomer undergo modification are analyzed in depth. Two series of PPAs substituted at the phenyl ring in *ortho*, *meta*, and *para* with either (*S*)-α-methoxy-α-phenylacetic acid (MPA) or (*S*)-phenylglycine methyl ester (PGME) linked through anilide or benzamide bonds were prepared (i.e., *o*-, *m*-, *p*-poly-**1** and poly-**2** series) and characterized both in solution and in the solid state (CD, UV−vis, Raman, NMR, DSC, TGA, X-ray, AFM, SEM). *Para*-substituted polymers (*p*-poly-**1** and *p*-poly-**2**) present the most compressed and dynamic helices, which respond easily to external stimuli. *Meta*-substituted PPAs (*m*-poly-**1** and *m*-poly-**2**) exist as a mixture in equilibrium of two different helices (compressed and stretched), both less dynamic than the *para* counterparts and with a weak response to external stimuli. Moreover, in the solid state, *m*-poly-**1** and *m*-poly-**2** show separate fields for the compressed and for the stretched helices. For its part, the *ortho*-substituted PPA (*o*-poly-**1**) presents a highly stretched, almost planar and practically rigid helical structure, inert to external stimuli and prone to aggregate. These structural changes (elongation/dynamic behavior) are rationalized on the basis of the increasing difficulties imposed by the *meta*- and *ortho*-substitution on the accommodation of the pendants within the helical structure.

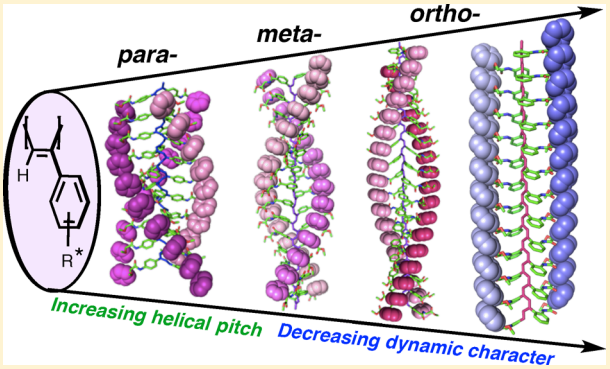

INTRODUCTION

Biopolymers such as peptides, polysaccharides, or DNA adopt helical structures, which are directly related to their function. This structural motif is responsible for the location of residues and functional groups at specific distances and orientations related to the sense and elongation of the helix. This spatial distribution determined by the helix is the critical factor in several important phenomena such as molecular recognition and catalysis, among others.

Based on this structure/function relationship, many synthetic polymers with helical structure [e.g., poly(phenylacetylene)s, poly(isocyanate)s, poly(isocyanide)s, poly(silane)s, poly(methyl methacrylate)s, etc.] have been developed and studied during the last decades.[1] In fact, the great majority of the more than five thousand papers published on this topic since 2000 have been centered on the discovery of new functional materials useful as sensors, as chiral recognition agents, as chiral chromatographic supports, as conductive devices, and so.

Interestingly, only in a few cases, the secondary helical structure of those polymers has been fully determined, and their helical sense, helical pitch, and packing angle known.

Poly(phenylacetylene)s[1,2] (PPAs) are a family of dynamic helical polymers[1] where the helical sense,[3] helical scaffold,[4] or both at the same time[5] can be tuned by the action of external stimuli. This property makes these materials very interesting for sensing,[6] chiral separations,[7] or asymmetric synthesis[8] and renders specially important to have a perfect knowledge of the structural parameters related to those functions.

Dynamic PPAs, i.e., PPAs devoid of chiral centers, exist in solution usually as mixtures in equilibrium of helices with opposite senses, that can shift to a preponderant helicity by the action of external stimuli.[1]

The conversion of those dynamic PPAs into nanostructured materials is essential for the development of stimuli responsive materials, and different approaches for the preparation of macroscopically helical nanoparticles, gels, 2D crystals, etc., have been described.[1,9]

From the stereochemical point of view, the transference of the mixed helices present in solution to the solid state is a particularly important process. So, assemblies made by either fields of mixed helical senses or separate domains for *P* and *M* helices can be obtained, leading to macroscopically racemic or chiral supramolecular entities, respectively.[1,10]

Received: May 10, 2016
Published: July 15, 2016

DOI: 10.1021/jacs.6b04834
J. Am. Chem. Soc. 2016, 138, 9620−9628

However, no exhaustive studies devoted to the role played by structural aspects such as the type of connectivity between the phenyl group and the molecular entities attached as pendants, that can affect the intramolecular hydrogen-bonding scaffold or the geometry of the substitution pattern at the phenyl group, in the case of disubstituted phenyls, are found in the literature of PPAs.

Most of the PPAs reported in literature are derived from *para*-substituted phenylacetylenes; and just very few have been reported with the pendants linked to the *meta*[11] and *ortho*[12] positions.

This distinction is important, not just because the steric interactions in *ortho* and *meta*-substituted monomers might prevent their polymerization, but more interesting because different substitution patterns (*ortho*, *meta*, or *para*) should lead to PPAs presenting different interactions among pendants that, in turn, would require also different helical adaptations in order to be stable.

This means that PPAs with the same pendant located in *ortho*, *meta*, or *para* might present helical skeletons with different dynamics, helical sense, elongation, conjugation and responses to external stimuli.

In *para*-substituted PPAs, it is known that the modification of the conformational composition of the pendants induces changes in the inter-[13] intrapendant interactions.[14] Therefore, a good knowledge of how the distinct connectivities and substitution patterns affect the pendant conformation could provide a way to correlate the pendant substitution with the resulting helical structure.

Here we describe how the type of linkage and substitution pattern in the monomer affects the helical skeleton of the polymer and how those changes can be used to tune the dynamic/static character of the helical scaffold as well as its degree of compression/stretching. These structural effects are observable either in solution or in the solid state and have a dramatic repercussion in the formation of 2D monolayers, in the response to stimuli (e.g., temperature, solvent effects, coordination with metal cations) and in the formation of supramolecular assemblies. All this information can be of utmost importance in future designs of helical PPAs.

To perform these studies, we carried out a comparison of the structure, in solution and solid state, of two series of PPAs: one bearing (*S*)-α-methoxy-α-phenylacetic acid [i.e., (*S*)-MPA; monomer M-**1**] and the other (S)-phenylglycine methyl ester [i.e., (*S*)-PGME; monomer M-**2**] as pendant groups, linked to the *o*-, *m*-, and *p*-positions through an anilide and a benzamide bond, respectively (Figure 1). These molecules were the pendants of choice due to their similar structures (i.e., they bear their chiral centers at the same bond distance and both have Ph and OMe substituents) and to their well-established conformational behaviors in solution. Furthermore, anilide and benzamide linkages—both involved in the intramolecular hydrogen-bonding framework—are the bonding types more used to connect side chains to the phenyl groups in PPAs.

Finally, another strong reason to choose these chiral pendants lies in the fact that the helical structures of their *para*-substituted PPAs (*p*-poly-**1** and *p*-poly-**2**, Figure 2) are sufficiently diverse in their dynamic character, sense preference, and compressed/stretched backbone, that they give a good starting point for comparison with their *meta* and *ortho* analogues.

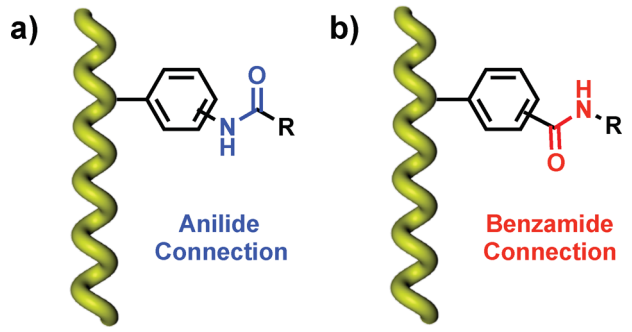

Figure 1. Schematic illustration of PPAs bearing the pendant groups attached through (a) anilide connections (monomers prepared from ethynylanilines and carboxylic acids) and (b) benzamide connections (monomers prepared from ethynylbenzoic acids and amines).

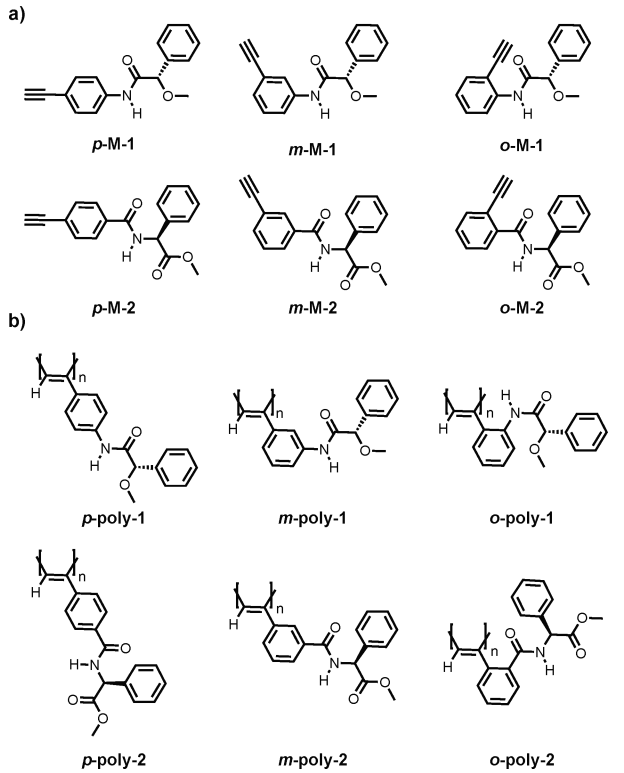

Figure 2. (a) Structures of *p*-M-**1**, *m*-M-**1**, *o*-M-**1**, *p*-M-**2**, *m*-M-**2**, and *o*-M-**2**. (b) Structures of *p*-poly-**1**, *m*-poly-**1**, *o*-poly-**1**, *p*-poly-**2**, *m*-poly-**2**, and *o*-poly-**2**.

RESULTS AND DISCUSSION

The *para*-, *meta*-, and *ortho*-ethynylanilides of (*S*)-α-methoxy-α-phenylacetic acid (i.e., *p*-M-**1**, *m*-M-**1**, *o*-M-**1**) and ethynylbenzamides of (*S*)-phenylglycine methyl ester (i.e., *p*-M-**2**, *m*-M-**2**, *o*-M-**2**) were synthesized (Figure 2a) and submitted to polymerization with $[\{Rh(nbd)Cl\}_2]$ (nbd = 2,5-norbornadiene) as catalyst affording PPAs *p*-poly-**1**, *m*-poly-**1**, *o*-poly-**1**, *p*-poly-**2**, and *m*-poly-**2** (Figure 2b).[15] All the synthesized polymers showed ^{1}H NMR (5.6−5.8 ppm) and Raman signals indicative of a *cis* polyene backbone (see SI).[16] Unfortunately, *o*-poly-**2** could not be obtained in spite of our efforts with different experimental conditions and catalysts. The structure of *o*-M-**2**, that shows a high degree of steric hindrance, impedes the polymerization (see below).

DOI: 10.1021/jacs.6b04834
J. Am. Chem. Soc. 2016, 138, 9620−9628

The Structure of *para*-Substituted Poly(phenylacetylene)s. Previous studies have shown that *p*-poly-**1** presents a dynamic helical structure in solution, with left- and right-handed helices in equal populations (e.g., null CD at 375 nm in $CHCl_3$, Figure 3a),[17] while *p*-poly-**2** adopts a single-handed helical structure (e.g., negative CD at 375 nm in $CHCl_3$) (Figure 3d).[18] These differences are related to the diverse conformations of both pendants. The MPA moiety found in *p*-poly-**1** exists in $CHCl_3$ as a 1:1 equilibrium between two conformers (sp, synperiplanar oriented carbonyl and methoxy groups; and ap, antiperiplanar oriented carbonyl and methoxy groups) that places the bulkiest group in orientations that favor a specific helical sense for each conformer (Figure 3a–c).[17]

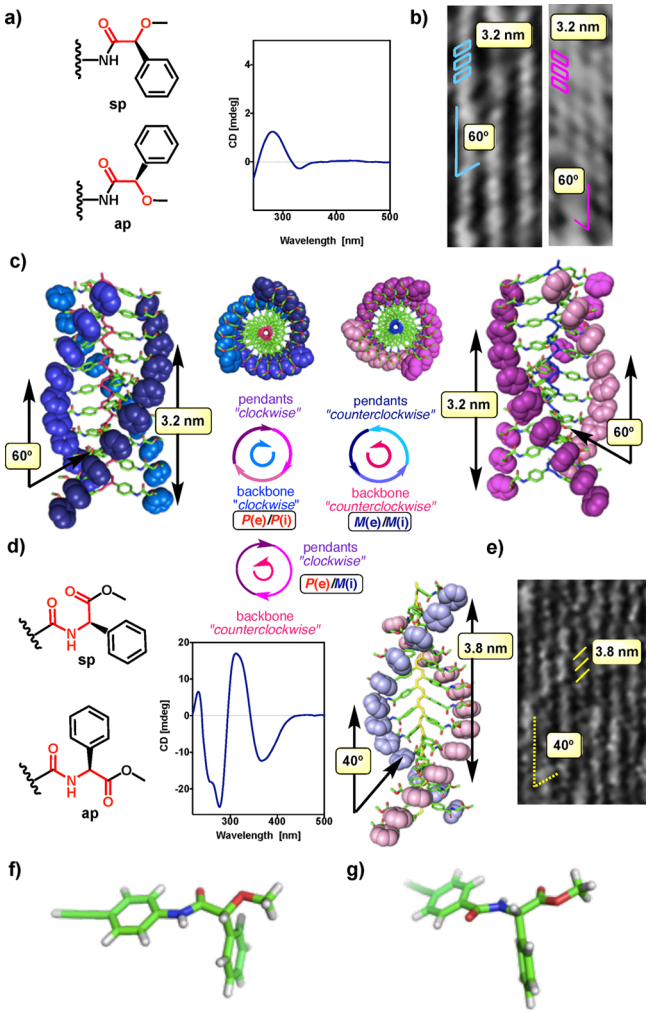

Figure 3. (a) Pendant conformations of *p*-poly-**1** and CD spectra in $CHCl_3$. (b) AFM images of right- and left-handed monolayers of *p*-poly-**1**. (c) 3D models of the structure of right- and left-handed helices of *p*-poly-1 and helicities of the external and internal helices (defined by the pendants and the polyene backbone, respectively). (d) Pendant conformations of *p*-poly-**2**, helicities of the external and internal helices, CD spectra in $CHCl_3$, and 3D model of the structure of the right-handed helix of *p*-poly-**2**. (e) AFM image of the right-handed monolayer of *p*-poly-**2**. (f) X-ray structure of monomer *p*-M-**1**. (g) X-ray structure of monomer *p*-M-**2**. For better understanding of the drawings and the identification of the functional groups involved in the helices, the phenyl rings of the pendants are represented as space-filling models.

For its part, the PGME group in *p*-poly-**2** exists in solution as a single preferred conformation that induces a predominant helical sense depending on the characteristics of the solvent (Figure 3d,e). For instance, in $CHCl_3$, the main conformation is ap (antiperiplanar oriented carbonyl groups; left-handed helix), while in DMSO, it is sp (synperiplanar oriented carbonyl groups; right-handed helix).[11]

In the solid state, *p*-poly-**1** generates AFM images indicating that the polymer adopts left- and right-handed compressed helices with a cis–cisoidal backbone (60°), three residues per turn and a helical pitch of 3.2 nm (Figure 3c).[10a] Those helices are found in independent fields formed by enantiomeric domains of *P* and *M* helical chains. For its part, *p*-poly-**2** presents, after AFM analysis, a preferred and stretched single cis–transoidal backbone (−158°), two residues per turn and a helical pitch of 3.8 nm (Figure 3d).[18]

When talking about the architecture of these polymers, it is interesting to point out a very important structural feature that is intrinsic to all helical PPAs and that usually is not sufficiently considered. Every PPA chain is always constituted by two "coaxial helices": external (defined by the pendants, detected by AFM) and internal (defined by the polyene backbone, detected by CD), and their respective helical senses can be coincident or not.

In the case of *p*-poly-**1**, the helicities of the external and internal helices of both "chains" are coincident [i.e., *M*(e)/*M*(i) and *P*(e)/*P*(i), Figure 3c], while in *p*-poly-**2**, they are opposite [i.e., *P*(e)/*M*(i), Figure 3d]. This is a general trend found in the helical PPAs we have studied due to the angles of their polyene backbone: 3/1 helices present the same helical sense in external and internal helices, while 2/1 helices present opposite senses.

In summary, PPAs substituted in the *para* position with chiral pendants and linked through either anilide or benzamide bonds afford 3/1 or 2/1 contracted helices, respectively, where the external or internal helices can show either the same (3/1) or opposite (2/1) helicities. All of them are able to undergo inversion or chiral amplification under the influence of appropriate stimuli due to the high degree of dynamic character they show (see below).[17,18]

Similar studies on the corresponding *meta* and *ortho*-substituted PPAs have been carried out and are described next.

The Structure of *meta*-Substituted Poly(phenylacetylene)s. After being synthesized (see SI), *m*-poly-**1** and *m*-poly-**2** were submitted to analysis both in solid-state and in solution. For the solid-state studies, a monolayer of *m*-poly-**1** on HOPG was prepared using a protocol based on the Langmuir–Schaeffer methodology[10a] and analyzed by high-resolution AFM. The images obtained of *m*-poly-**1** showed well-ordered polymer chains, packed in a parallel fashion. Interestingly, the monolayer presents separate regions homogeneously formed by stretched and by compressed helical scaffolds, but no areas of mixed packing were found (Figure 4). Thus, the behavior of this *meta* polymer differs from that shown by its *para* analog, where the two observed scaffolds showed compressed 3/1 structures (Figure 3b,c).

The compressed helix presents a 3.2 nm helical pitch and 60° packing angle. These values are similar to those reported for *p*-poly-**1** that has a contracted helix with a cis–cisoidal backbone (+60°) and three residues per turn (Figures 3c and 4a).

On the other hand, the stretched helix presents 5.3 nm helical pitch and 40° packing angle that by modeling corresponds to a cis–transoidal (+160°) helix with two residues per turn (Figure 4b).

DOI: 10.1021/jacs.6b04834
J. Am. Chem. Soc. 2016, 138, 9620–9628

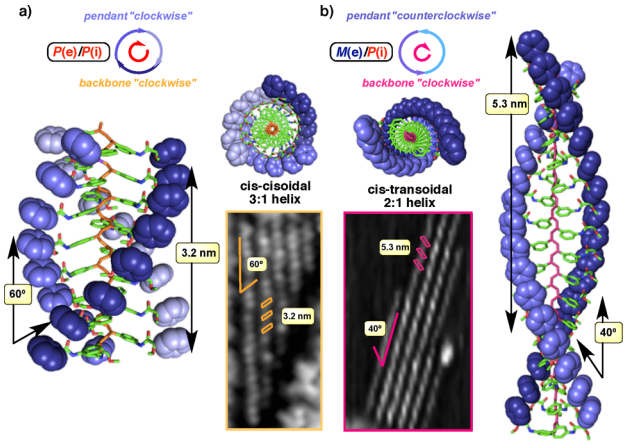

Figure 4. (a) AFM image, helicities of the external and internal helices and 3D model of the compressed (cis−cisoidal) structure of *m*-poly-**1**. (b) Idem of the stretched (cis−transoidal) structure of *m*-poly-**1**.

In the case of *m*-poly-**1**, the backbone of contracted and stretched helices rotates in the same *P* sense, internal helices, (+60°, + 160° respectively; same CD sign at 375 nm), while the external helices rotate in opposite senses: *P* for the contracted chain and *M* for the stretched one [i.e., *P*(e)/*P*(i) contracted; *M*(e)/*P*(i) stretched, Figure 4]. Both helices can accommodate the pendants in an ap conformation, a structural array also found in the monomer *m*-M-**1** both in solid state (X-ray, Figure 5c) and in solution (CD studies, see SI).

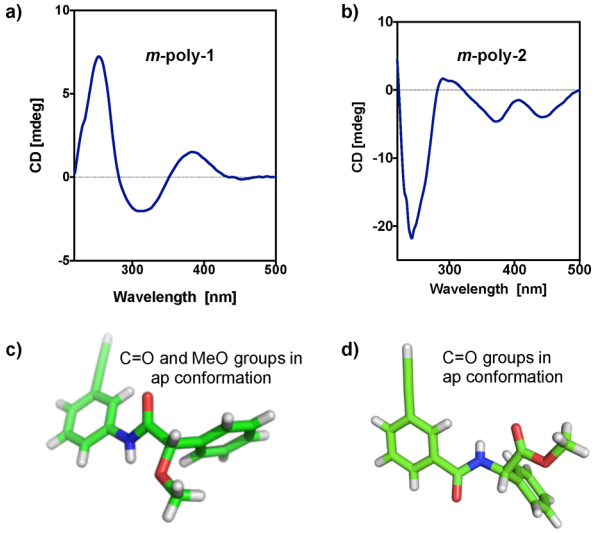

Figure 5. (a) CD spectrum of *m*-poly-**1**. (b) CD spectrum of *m*-poly-**2**. (c) X-ray structure of monomer *m*-M-**1**. (d) X-ray structure of monomer *m*-M-**2**.

The structure inferred for *m*-poly-**1** in THF solution is in agreement with the presence of those two types of helices in equilibrium. The CD presents a very strong positive band at around 240 nm (band in part associated with the pendant conformation, 3rd Cotton effect) and two smaller bands centered at 320 nm (negative) and 400 nm (positive) in the polyene region (first and second Cotton effects respectively, Figure 5a). In addition, when the CD spectra were recorded at different temperatures (Figure 6a), the intensities of the two polyene bands evolve as expected for an equilibrium mixture between (a) a more stable contracted helix (i.e., cis−cisoid, 3/1), that increases both its population and band intensities (first and second Cotton effects) at lower temperatures and (b) a less stable stretched one (i.e., cis−transoid, 2/1), that increases its population at higher temperatures together with a smaller contribution to the band intensities. In accordance with this, the UV band of *m*-poly-**1** at 400 nm suffers a hypsochromic shift when temperature decreases (smaller polyene conjugation, cis−cisoid) and a bathochromic shift at higher temperatures (larger polyene conjugation, cis−transoid; Figure 6b).

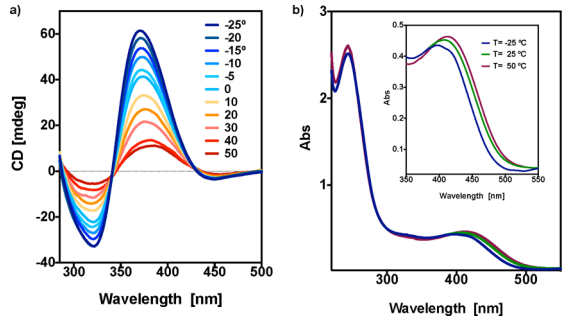

Figure 6. (a) VT-CD of *m*-poly-**1** showing the variations of the first and second Cotton effects at different temperatures (from −25 to +50 °C). (b) VT-UV of *m*-poly-**1** showing the hypsochromic/bathochromic shifts as temperature decreases/increases (from −25 to +50 °C). CD and UV spectra were recorded in THF at 0.3 mg/mL.

In resume, the structure of *m*-poly-**1** is characterized by the coexistence, both in solid state and in solution, of stretched (i.e., 2/1) and compressed (i.e., 3/1) helical scaffolds, formed in both cases by a *cis*-polyene skeleton. DSC and Raman studies confirmed the presence of *cis*-polyene structures in *m*-poly-**1** (see SI).

To our knowledge, this is the first time that a PPA is reported having different types of helical chains (cis−cisoidal 3/1 and cis−transoidal 2/1) both in solid state and in solution.

Similarly, monolayers of *m*-poly-**2** were deposited on HOPG as before and submitted to high-resolution AFM. The images indicated the presence of well-ordered 2D crystals, with the polymer chains packed in a parallel fashion (Figure 7).

Two different types of assemblies are distinguished. In one of them, the chains show a helical pitch of 3.8 nm and a packing angle of 40°. Modeling (Figure 7a) based on these values leads to a helix with a cis−transoidal backbone (i.e., 158°) and two

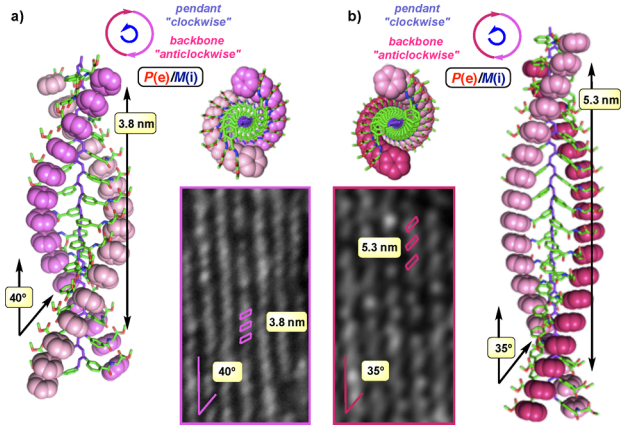

Figure 7. (a) 3D structure and AFM image for the compressed structure of *m*-poly-**2**. (b) 3D structure and AFM image for the stretched structure of *m*-poly-**2**.

DOI: 10.1021/jacs.6b04834
J. Am. Chem. Soc. 2016, 138, 9620−9628

residues per turn similar to the helix of *p*-poly-**2** (2/1, Figure 3d).

The other assembly showed by AFM helices with 5.3 nm pitch and 35° packing angle that corresponds, by modeling, also to a cis−transoidal (i.e., 165°) polyene backbone describing a helix with two residues per turn (2/1, Figure 7b). Raman spectra of *m*-poly-**2** (film, $CHCl_3$) showed bands in the *cis*-C−H region at 995 and 1004 cm^{-1}, corroborating the existence of those two cis−transoidal helical scaffolds. As in the case of *m*-poly-**1**, both helices show pendants in ap conformation, as it also happens in monomer *m*-M-**2** both in solid state (X-ray, Figure 5d) and in solution (CD studies, see SI).

In solution, *m*-poly-**2** shows a CD spectrum with two negative bands in the polyenic region (i.e., 365 and 442 nm) and a UV both coherent with the presence of two helices, one more compressed (negative CD band at 365 nm, similar to *p*-poly-**2**) than the other (442 nm) (Figure 8a).

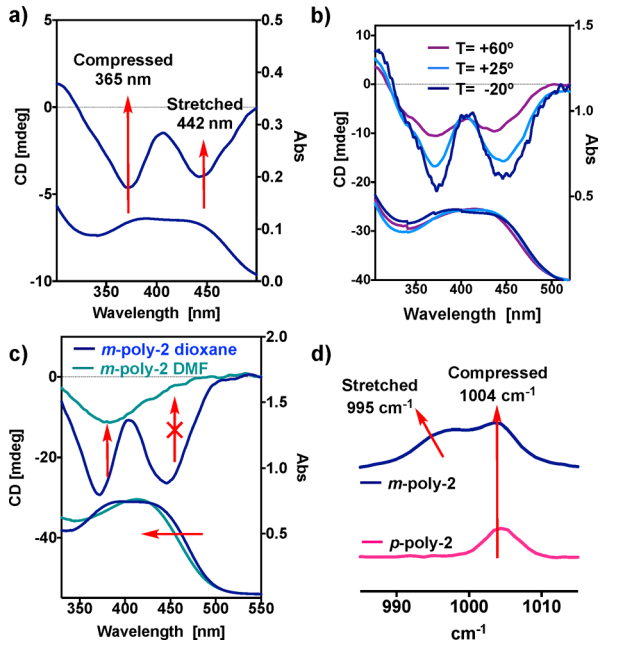

Figure 8. (a) CD and UV spectra of *m*-poly-**2** in dioxane showing two bands in both spectra indicating the presence of compressed and stretched helical structures. (b) VT-CD and VT-UV of *m*-poly-**2** in dioxane showing decreasing CD signals as temperature increases, but maintaining the ratio between stretched and compressed helices. (c) CD and UV spectra of *m*-poly-**2** in dioxane and DMF. CD shows the decrease of the stretched helix (the band at 442 nm almost disappears). UV shows a hypsochromic shift in fully agreement with the disappearance of the CD band at 442 nm. (d) Overlay of Raman spectra of *p*-poly-**2** and *m*-poly-**2**, showing the compressed helix (1004 cm^{-1}) in the former and the coexistence of stretched and compressed helices in the latter (995 and 1004 cm^{-1} respectively).

Recording the CD spectra at different temperatures in dioxane (VT-CD) shows that the two polyene bands undergo similar variations, thus suggesting that the two helices are virtually in a 1:1 equilibrium (Figure 8b). As expected, VT-UV recording did not show significant hypso or bathochromic effects in that solvent either (Figure 8b).

Information about dynamic/static character of the helical scaffold of *m*-poly-**2** was obtained observing the changes produced in solvents of different polarity. Thus, when the CD of *m*-poly-**2** was recorded in polar solvents such as DMF or DMSO, the band due to the more conjugated (stretched) polyene (442 nm) diminishes its intensity, almost disappearing, while the band due to the less conjugated helix (365 nm) increases. Similarly, the UV showed in polar solvents a significant hypsochromic effect on the vinylic band (Figure 8c), coherent with the expected decrease in conjugation that is expected for a more contracted polyene scaffold.

In summary, *m*-poly-**2** is composed by two types of cis−transoidal helices (i.e., 2/1) that differ from each other in their degree of elongation. In solid state they form separate monolayer fields, while in solution they are in equilibrium between the compressed and stretched forms. Resorting to solvents of different polar and donor properties can shift this equilibrium.

It is noteworthy to highlight how small changes in the polyene dihedral angle (from 158° to 165°) produce large structural changes observable not only in the AFM images (e.g., the helical pitch) but also in the CD-UV spectra (e.g., the different absorptions at the vinylic region). The larger conjugation between the double bonds in the stretched helices when compared to the compressed ones justifies the bathochromic effect observed in the former.

The Structure of *ortho*-Substituted Poly(phenylacetylene)s. The *ortho*-substituted monomers *o*-M-**1** and *o*-M-**2** were submitted to polymerization as above, but in spite of our efforts and numerous changes in experimental conditions and the use of different Rh(I) catalysts, *o*-M-**2** could not be converted into the corresponding polymer (see explanation below), forcing us to continue the work with *o*-poly-**1** as the only representative of *ortho*-substituted polymer. This polymer was isolated as a dark red material with a poor solubility in common organic solvents.

2D crystals of *o*-poly-**1** were prepared by spin-coating[10b−g] (see SI), and when their AFM images on HOPG were examined, surprisingly they did not show the presence of single chains, but extended left-handed helical fibers with a helical pitch of 13 nm, a packing angle of 40° (Figure 9a), and diameters in a range of 6−15 nm, indicating that they are formed by self-assembly of individual polymer chains. The height of these fibers corresponds to the diameter of a single chain (2 nm) (Figure 9b).

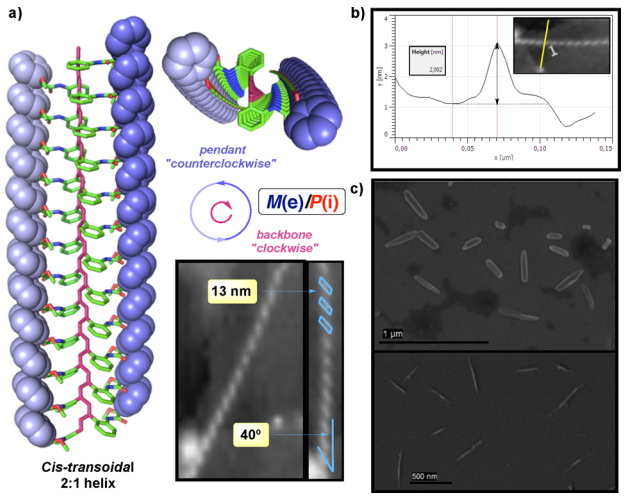

Figure 9. (a) 3D model and AFM image of *o*-poly-**1** fibers. (b) Cross section of a fiber (13 nm wide) showing its height (2 nm). (c) SEM images of larger chiral nanostructures formed by the supramolecular assembly of *o*-poly-**1**.

DOI: 10.1021/jacs.6b04834
J. Am. Chem. Soc. 2016, 138, 9620−9628

With the aforementioned data on hand, we carried out structure modeling and found a perfect match with a polyene structure with a cis−transoidal helical backbone (+175°, 2/1) describing a *P* internal helix while the pendants describe a *M* external helix [i.e., *M*(e)/*P*(i)], generating an almost planar structure. The pendants show an ap arrangement, that is also found in monomer *o*-M-**1** in solid state (X-ray, Figure 10b) and

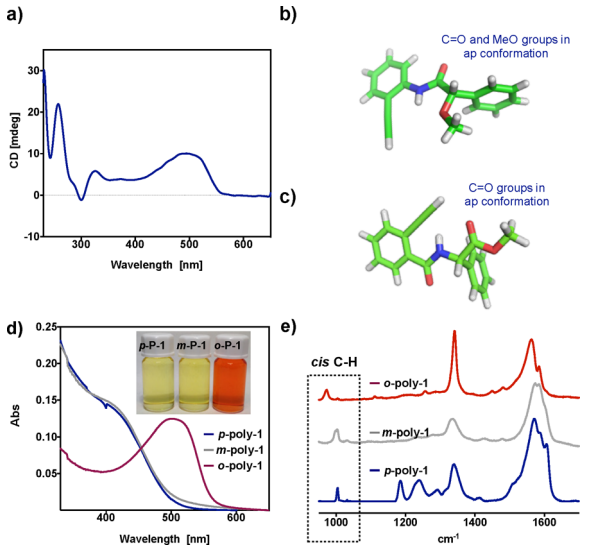

Figure 10. (a) CD spectra of *o*-poly-**1**. (b) CD and X-ray structure of *o*-M-**1**. (c) CD and X-ray structure of *o*-M-2. (d) Overlay of UV spectra (0.1 mg/mL $CHCl_3$) of *p*-poly-**1**, *m*-poly-**1**, and *o*-poly-**1** showing the bathochromic shift of the last one at the vinylic region. A picture of vials containing solutions of the corresponding polymers in $CHCl_3$ to perceive the change of color has been inserted. (e) Raman spectra of *p*-poly-**1**, *m*-poly-**1** and *o*-poly-**1** highlighting the *cis*-C−H band. A shift toward lower wavelength is observed in *o*-poly-**1**.

in solution (CD studies, see SI). The X-ray structure clearly shows the short distance between the pendant and the alkyne group that is even shorter in *o*-M-**2** (Figure 10c). This last fact justifies the lack of reactivity of *o*-M-**2** with the Rh(I) catalysts.

Raman spectra corroborated the *cis*-polyene skeleton with a C−H band at 973 cm^{-1}. In fact, this frequency is much lower than in the *meta* and *para* counterparts (995 and 1004 cm^{-1}, respectively), clearly indicating that the helical backbone of *o*-poly-**1** is much more stretched (Figure 10e).

Moreover, when this extended structure is examined, it shows the hydrophobic constituents (i.e., Ph groups, the polyene scaffold) much more exposed to the solvent than in the case of the *para* or *meta* analogues. This structural feature, together with the large degree of planarity reached by the polyene system that facilitates the docking between nearby chains, can explain the high tendency of *o*-poly-**1** to form fibers by aggregation. In fact, this capacity for aggregation can be tuned by adequate selection of solvent and concentrations, to produce chiral fibers with different lengths, diameters and shapes.

For instance, while a 0.01 mg/mL solution of *o*-poly-**1** in chloroform forms by spin-coating just fibers of 13 nm on HOPG (Figure 9a), the slow evaporation of a solution 0.1 mg/mL in an 8:2 chloroform/butanone mixture on silicon wafer by drop-casting led to the formation of larger chiral fibrillar aggregates with diameters around 25 nm and different lengths (from 100 to 500 nm, fiber-like). These fibers seem to be an intermediate aggregation state that leads to the formation of even larger rod-like structures with a width of 55−60 nm and variable lengths ranging from 100 nm to 4.3 μm (Figures 9c and 11). It is necessary to point out that the width of the aggregates, also observed in THF solutions, seems to follow a well-defined growth pattern in which the width of one aggregate doubles approximately the width of the previous one (i.e., 13, 25, 60; Figure 11).

The highly stretched helical structure observed in the solid phase is also present in solution, where *o*-poly-**1** shows the CD polyenic band at 508 nm (a bathochromic shift of about 100 nm when compared to the corresponding bands in the *para* and *meta* analogues, Figure 10a) and a dark-red color, with UV

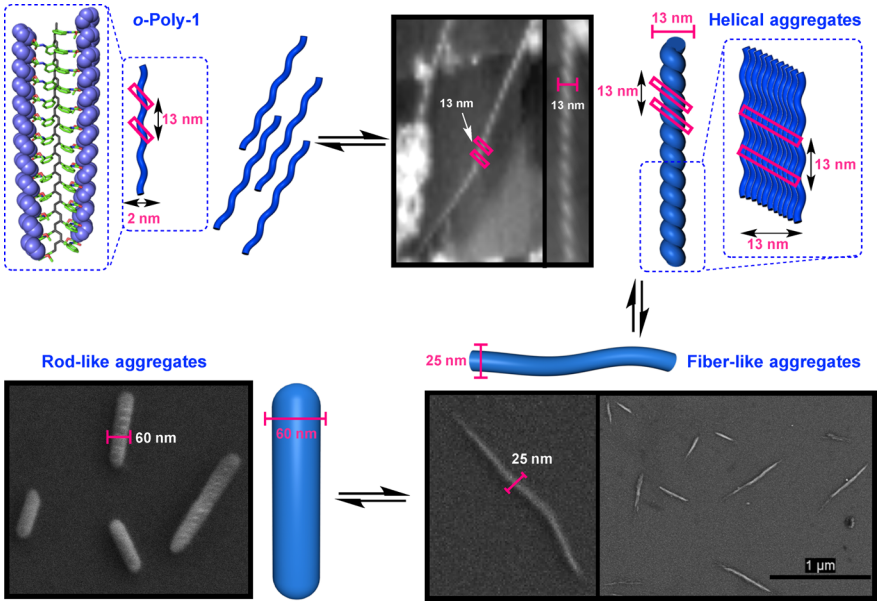

Figure 11. Evolution of *o*-poly-**1** aggregates from single chains to complex chiral nanostructures formed by the supramolecular assembly of *o*-poly-**1**. AFM and SEM images of the different types of aggregates are also shown.

DOI: 10.1021/jacs.6b04834
J. Am. Chem. Soc. 2016, 138, 9620−9628

maximum at 508 nm illustrative of an almost planar and highly conjugated cis−transoid polyene (Figure 10d). *o*-Poly-**1** is so rigid that no changes on the helical sense or pitch can be observed by interaction with metal ions or polar solvents, therefore it can be defined as a quasi-static helical polymer.

In summary, *o*-poly-**1** presents both in solution and in the solid state a single type of cis−transoidal chain characterized by its long helical pitch, a nearly planar and rigid shape, and a large degree of conjugation. These structural features and the external position of the hydrophobic groups explain the tendency of this polymer to form fibrillar aggregates of different sizes and shapes, a phenomenon that was not observed in the other polymers described in this work.

The Role Played by the Connectivity and the Substitution Pattern in PPA Architecture. It has been shown in many *para*-substituted dynamic PPAs, both with anilide or benzamide links, that the conformational composition of the pendants determines the preference for a certain helical sense and pitch of the helix.[1,10,13,14,17,18] For instance, in *p*-poly-**1**, an equal ratio of two conformers of MPA leads to an equal proportion of cis−cisoid *P* and *M* helices (3/1); in *p*-poly-**2**, the PGME pendant has an excess of one conformer, and therefore, the polymer shows an excess of one helical sense (cis−transoid *P* or *M*, 2/1, see above). In both cases, the helices can be classified as compressed ones (Figure 12).

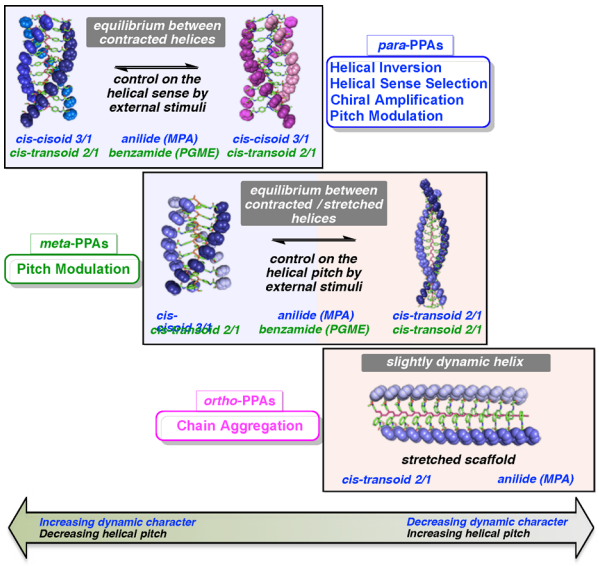

Figure 12. Types of PPA scaffolds according to the connectivity/pattern of substitution and main responses to external stimuli.

In solution, the helices of the *para* polymers are highly dynamic and respond effortlessly to external stimuli. Thus, when variations in temperature, in the polarity and the donor/acceptor character of the solvent, or by the addition of metal ions with different valence (mono and di) modify the conformational composition of the pendants, the polymeric backbones act as sensors that respond in a number of ways: inverting the helical sense (helical inversion), selective shifting to one sense or the other (helical selection), stretching or shortening of the chains (pitch modulation), and increasing the optical response mediated by domino or Sergeants and Soldiers effects (chiral amplification).

In contrast, when those very same pendants are located in *meta* position instead of *para*, the polymers show the presence of two scaffolds in equilibrium: a compressed helix (cis−cisoid, 3/1, in *m*-poly-**1**; cis−transoid, 2/1, in *m*-poly-**2**) and a stretched helix (cis−transoid, 2/1, in *m*-poly-**1**; cis−transoid, 2/1, in *m*-poly-**2**).

Interestingly, the compressed helices in both cases are structurally similar to the compressed ones found in their *para* counterparts, being the stretched chains the ones that differ from those found in the *para* polymers.

The equilibria between compressed and stretched helices in the *meta* polymers can be partially modulated by temperature or solvents but never to the degree reached in the *para* polymers. Furthermore, they do not undergo significant changes either under the action of metal cations (see SI). Consequently, with the *meta* PPAs, phenomena such as helical inversion (with solvents or metal cations) or helical selection (with metal cations) are not possible (see SI).

Finally, the *ortho* polymer, available only through an anilide bond, shows the largest and single stretched helix (cis−transoid, 2/1) and a quasi-static behavior that prevents any kind of modulation by external stimuli (solvents, cations, see SI). However, its stiffness and close-to-planar structure produce a new effect not observable in the other polymers: They facilitate the aggregation between chains that leads to the formation of supramolecular assemblies in the form of fibers or rod-like nanostructures (Figure 12).

CONCLUSIONS

In summary, we have demonstrated how mutations on the aromatic substitution pattern—*para*, *meta*, and *ortho*—and connectivity—anilide, benzamide—of a chiral PPA affect its helical scaffold and dynamic behavior and consequently the response to external stimuli. Thus, when the chiral pendant group gets closer to the polyene backbone (when going from *para* to *meta* and to *ortho*-substituted PPAs), the polymer releases the generated steric hindrance by elongation of the polymer chain. Interestingly, we found that in *meta*-substituted PPAs (*m*-poly-**1** and *m*-poly-**2**), where the pendant moiety is located in-between the *para* and the *ortho* position, the PPAs present in solution an equilibrium between two different helical structures, one similar to that observed in the *para* analogue, and another more stretched one. AFM images showed that those two helices generate, in the solid state, two different domains of 2D-crystals specific for each helix. The internal sense of the two helices is the same (e.g., left handed), but the helix described by the pendants can be identical (in *m*-poly-**1**) or opposite (*m*-poly-**2**) to the internal helix, depending on the elongation of the polyene backbone.

On the other hand, the *ortho*-substituted polymer (*o*-poly-**1**) has the pendant group so close to the backbone that in order to release the steric hindrance, it adopts an almost planar structure. The presence of this flattered structure leads to the aggregation of the polymer chains, through the hydrophobic PPA backbone resulting in the formation of chiral fibers with different sizes, as observed by AFM and SEM experiments.

In addition, these studies also demonstrate that going from *para* to *meta* and to *ortho* substitution affects the dynamic behavior of the polyene chain. Thus, while *para*-substituted PPAs (*p*-poly-**1** and *p*-poly-**2**) are highly flexible and respond easily to the polarity and donor character of solvents or to metal ions, *ortho*-substituted PPAs as *o*-poly-**1**, form quasi-static helices, whose helical sense cannot be tuned by external stimuli due to the restricted conformation at the pendant moiety.

DOI: 10.1021/jacs.6b04834
J. Am. Chem. Soc. 2016, 138, 9620−9628

With regard to the *meta*-substituted polymers (*m*-poly-**1** and *m*-poly-**2**), their helices can be slightly tuned by external stimuli that act on the conformational composition of the pendants, shift the equilibrium between the two helices but never to the high degree of response reached with their *para* counterparts (Figure 12).

Thus, we believe that the substitution patterns discussed in this work can be used as a very efficient tool to obtain helical PPAs with the desired degree of stretching, dynamism, and response to external stimuli. Moreover, these findings provide very useful information about the structure of these PPAs and their function as sensors, chiral stationary phases, chiral ligands for asymmetric synthesis, etc.

The coexistence in the structure of PPAs of internal and external (2/1 or 3/1) helices that can rotate in the same or opposite senses, that are detected by different techniques (CD for the internal helix and AFM for the external one), found in different states (solution, film, 2D crystal) and the relevance of their interplay, should be stressed. This stereochemical aspect is particularly important when the PPA or the derived nanostructures are aimed to the development of macroscopically chiral supports, catalysts, sensors, or nanoreactors, because in these cases, only the external helix is relevant.

■ ASSOCIATED CONTENT

Supporting Information

The Supporting Information is available free of charge on the ACS Publications website at DOI: 10.1021/jacs.6b04834.

Materials and methods; synthesis of monomers; CD studies of monomers; synthesis of polymers; GPC studies; circular dichroism and ultraviolet studies; thermal studies; AFM studies; response of the polymers to external stimuli: solvents and metal cations; supporting references (PDF)
Crystallographic data (ZIP)

■ AUTHOR INFORMATION

Corresponding Authors

*ricardo.riguera@usc.es
*felix.freire@usc.es

Notes

The authors declare no competing financial interest.

■ ACKNOWLEDGMENTS

We thank Servicio de Nanotecnología y Análisis de Superficies (CACTI, UVIGO). R.R. and F.F. thank MEC for a FPI contract and a Ramón y Cajal contract, respectively. This work was supported by grants from MEC (CTQ2014-61470-EXP, CTQ2015-70519-P) and Xunta de Galicia (GRC2014/040, EM2013/0032). Ministerio de Economía y Competitividad (MEC), European Regional Development Fund (ERDF), and Xunta de Galicia are acknowledged.

■ REFERENCES

(1) (a) Simionescu, C. I.; Percec, V. *J. Polym. Sci., Polym. Symp.* **1980**, *67*, 43. (b) Green, M. M.; Peterson, N. C.; Sato, T.; Teramoto, A.; Cook, R.; Lifson, S. *Science* **1995**, *268*, 1860. (c) Gellman, S. H. *Acc. Chem. Res.* **1998**, *31*, 173. (d) Nielsen, P. E. *Acc. Chem. Res.* **1999**, *32*, 624. (e) Nakano, T.; Okamoto, Y. *Chem. Rev.* **2001**, *101*, 4013. (f) Hill, D. J.; Mio, M. J.; Prince, R. B.; Hughes, T. S.; Moore, J. S. *Chem. Rev.* **2001**, *101*, 3893. (g) Cornelissen, J. J. L. M.; Rowan, A. E.; Nolte, R. J. M.; Sommerdijk, N. A. J. M. *Chem. Rev.* **2001**, *101*, 4039. (h) Fujiki, M. *Macromol. Rapid Commun.* **2001**, *22*, 539. (i) Nomura, R.; Nakako, H.; Masuda, T. J. *J. Mol. Catal. A: Chem.* **2002**, *190*, 197. (j) Fujiki, M.; Koe, J. R.; Terao, K.; Sato, T.; Teramoto, A.; Watanabe, J. *Polym. J.* **2003**, *35*, 297. (k) Huc, I. *Eur. J. Org. Chem.* **2004**, *2004*, 17. (l) Sugimone, M.; Ito, Y. *Advances in Polymer Science*; Springer: Berlin, 2004; Vol. *171*, p 77 (m) Lam, J. W. Y.; Tang, B. Z. *Acc. Chem. Res.* **2005**, *38*, 745. (n) Maeda, K.; Yashima, E. *Top. Curr. Chem.* **2006**, *265*, 47. (o) Amabilino, D. B.; Serrano, J. L.; Sierra, T.; Veciana, J. *J. Polym. Sci., Part A: Polym. Chem.* **2006**, *44*, 3161. (p) Yashima, E.; Maeda, K. In *Foldamers: Structure, Properties, and Applications*; Hecht, S., Huc, I., Eds.; Wiley-VCH: Weinheim, 2007; pp 331. (q) Fujiki, M. *Top. Curr. Chem.* **2007**, *284*, 119. (r) Yashima, E.; Maeda, K.; Furusho, Y. *Acc. Chem. Res.* **2008**, *41*, 1166. (s) Pijper, D.; Feringa, B. L. *Soft Matter* **2008**, *4*, 1349. (t) Rudick, J. G.; Percec, V. *Acc. Chem. Res.* **2008**, *41*, 1641. (u) Yashima, E.; Maeda, K.; Iida, H.; Furusho, Y.; Nagai, K. *Chem. Rev.* **2009**, *109*, 6102. (v) Rosen, B. M.; Wilson, C. J.; Wilson, D. A.; Peterca, M.; Imam, M. R.; Percec, V. *Chem. Rev.* **2009**, *109*, 6275. (w) Iida, H.; Yashima, E. *Synthesis and Application of Helical Polymers with Macromolecular Helicity Memory, in Polymeric Chiral Catalyst Design and Chiral Polymer Synthesis*, ed. Itsuno, S., John Wiley & Sons, Hoboken, NJ, USA, 2011, ch. 7, p 201. (x) Schwartz, E.; Koepf, M.; Kitto, H. J.; Nolte, R. J. M.; Rowan, A. E. *Polym. Chem.* **2011**, *2*, 33. (y) Le Bailly, B. A. F.; Clayden, J. *Chem. Commun.* **2016**, *52*, 4852. (z) Yu, Z.; Hecht, S. *Chem. Commun.* **2016**, *52*, 6639.

(2) (a) Freire, F.; Quiñoá, E.; Riguera, R. *Chem. Rev.* **2016**, *116*, 1242. (b) Rudick, J. *Adv. Polym. Sci.* **2013**, *262*, 345. (c) Freire, F.; Seco, J. M.; Quiñoá, E.; Riguera, R. *Adv. Polym. Sci.* **2013**, *262*, 123. (d) Li, W.-S.; Aida, T. *Chem. Rev.* **2009**, *109*, 6047. (e) Yashima, E.; Maeda, K. *Macromolecules* **2008**, *41*, 3. (f) Percec, V.; Rudick, J. G.; Peterca, M.; Heiney, P. A. *J. Am. Chem. Soc.* **2008**, *130*, 7503. (g) Rudick, J. G.; Percec, V. *New J. Chem.* **2007**, *31*, 1083.

(3) Hu, Y.; Liu, R.; Sanda, F.; Masuda, T. *Polym. J.* **2008**, *40*, 143.

(4) (a) Percec, V.; Rudick, J. G.; Peterca, M.; Wagner, M.; Obata, M.; Mitchell, C. M.; Cho, W.-D.; Balagurusamy, V. S. K.; Heiney, P. A. *J. Am. Chem. Soc.* **2005**, *127*, 15257. (b) Percec, V.; Aqad, E.; Peterca, M.; Rudick, J. G.; Lemon, L.; Ronda, J. C.; De, B. B.; Heiney, P. A.; Meijer, E. W. *J. Am. Chem. Soc.* **2006**, *128*, 16365. (c) Percec, V.; Rudick, J. G.; Peterca, M.; Aqad, E.; Imam, M. R.; Heiney, P. A. *J. Polym. Sci., Part A: Polym. Chem.* **2007**, *45*, 4974. (d) Percec, V.; Peterca, M.; Rudick, J. G.; Aqad, E.; Imam, M. R.; Heiney, P. A. *Chem. - Eur. J.* **2007**, *13*, 9572.

(5) (a) Yashima, E.; Maeda, K.; Sato, O. *J. Am. Chem. Soc.* **2001**, *123*, 8159. (b) Maeda, K.; Kamiya, N.; Yashima, E. *Chem. - Eur. J.* **2004**, *10*, 4000. (c) Zhao, H. C.; Sanda, F.; Masuda, T. *J. Polym. Sci., Part A: Polym. Chem.* **2005**, *43*, 5168. (d) Zhao, H. C.; Sanda, F.; Masuda, T. *Macromol. Chem. Phys.* **2005**, *206*, 1653. (e) Sanda, F.; Terada, K.; Masuda, T. *Macromolecules* **2005**, *38*, 8149. (f) Maeda, K.; Mochizuki, H.; Watanabe, M.; Yashima, E. *J. Am. Chem. Soc.* **2006**, *128*, 7639.

(6) (a) Anger, E.; Iida, H.; Yamaguchi, T.; Hayashi, K.; Kumano, D.; Crassous, D.; Vanthuyne, N.; Rousselc, C.; Yashima, E. *Polym. Chem.* **2014**, *5*, 4909. (b) Iida, H.; Miki, M.; Iwahana, S.; Yashima, E. *Chem. - Eur. J.* **2014**, *20*, 4257.

(7) Shimomura, K.; Ikai, T.; Kanoh, S.; Yashima, E.; Maeda, K. *Nat. Chem.* **2014**, *6*, 429.

(8) (a) Megens, R. P.; Roelfes, G. *Chem. - Eur. J.* **2011**, *17*, 8514. (b) Tang, Z.; Iida, H.; Hu, H.-Y.; Yashima, E. *ACS Macro Lett.* **2012**, *1*, 261. (c) Iida, H.; Tang, Z.; Yashima, E. *J. Polym. Sci., Part A: Polym. Chem.* **2013**, *51*, 2869.

(9) (a) Rudick, J. G.; Percec, V. *Macromol. Chem. Phys.* **2008**, *209*, 1759. (b) Lam, J. W. Y.; Tang, B. Z. *J. Polym. Sci., Part A: Polym. Chem.* **2003**, *41*, 2607.

(10) (a) Rodríguez, R.; Ignés-Mullol, J.; Sagués, F.; Quiñoá, E.; Riguera, R.; Freire, F. *Nanoscale* **2016**, *8*, 3362. (b) Ohsawa, S.; Sakurai, S.-I.; Nagai, K.; Banno, M.; Maeda, K.; Kumaki, J.; Yashima, E. *J. Am. Chem. Soc.* **2011**, *133*, 108. (c) Yashima, E. *Polym. J.* **2010**, *42*, 3. (d) Sakurai, S.-I.; Ohsawa, K.; Nagai, K.; Okoshi, K.; Kumaki, J.; Yashima, E. *Angew. Chem., Int. Ed.* **2007**, *46*, 7605. (e) Okoshi, K.; Sakurai, S.; Ohsawa, J. K.; Yashima, E. *Angew. Chem., Int. Ed.* **2006**, *45*, 1245. (f) Sakurai, S.-I.; Okoshi, K.; Kumaki, J.; Yashima, E. *J. Am.*

DOI: 10.1021/jacs.6b04834
J. Am. Chem. Soc. 2016, 138, 9620−9628

Chem. Soc. **2006**, *128*, 5650. (g) Nishimura, T.; Takatani, K.; Sakurai, S.; Maeda, K.; Yashima, E. *Angew. Chem., Int. Ed.* **2002**, *41*, 3602.
(11) (a) Liu, L.; Long, Q.; Aoki, T.; Zhang, G.; Kaneko, T.; Teraguchi, M.; Zhang, Ch.; Wang, Y. *Chirality* **2015**, *27*, 454. (b) Maeda, K.; Morioka, k.; Yashima, E. *Macromolecules* **2007**, *40*, 1349. (c) Goto, H.; Morino, K.; Morishita, T.; Maeda, K.; Yashima, E. *Kobunshi Ronbunshu* **2006**, *63*, 325. (d) Maeda, K.; Okada, S.; Yashima, E.; Okamoto, Y. *J. Polym. Sci., Part A: Polym. Chem.* **2001**, *39*, 3180. (e) Karim, S. M. A.; Nomura, R.; Masuda, T. *Polym. Bull.* **1999**, *43*, 305. (f) Yashima, E.; Maeda, Y.; Matsushima, T.; Okamoto, Y. *Chirality* **1997**, *9*, 593.
(12) (a) Pauly, A. C.; Theato, P. *Macromol. Rapid Commun.* **2013**, *34*, 516. (b) Katsumata, T.; Shiotsuki, M.; Sanda, F.; Sauvage, X.; Delaude, L.; Masuda, T. *Macromol. Chem. Phys.* **2009**, *210*, 1891. (c) Mayershofer, M. G.; Wagner, M.; Anders, U.; Nuyken, O. *J. Polym. Sci., Part A: Polym. Chem.* **2004**, *42*, 4466. (d) Kunzler, J.; Percec, V. *J. Polym. Sci., Part A: Polym. Chem.* **1990**, *28*, 1221.
(13) (a) Leiras, S.; Freire, F.; Seco; Quiñoá, E.; Riguera, R. *Chem. Sci.* **2015**, *6*, 246. (b) Leiras, S.; Freire, F.; Seco, J. M.; Quiñoá, E.; Riguera, R. *Chem. Sci.* **2013**, *4*, 2735.
(14) (a) Arias, S.; Bergueiro, J.; Freire, F.; Quiñoá, E.; Riguera, R. *Small* **2016**, *12*, 238. (b) Bergueiro, J.; Freire, F.; Wendler, E. P.; Seco, J. M.; Quiñoá, E.; Riguera, R. *Chem. Sci.* **2014**, *5*, 2170. (c) Arias, S.; Freire, F.; Quiñoá, E.; Riguera, R. *Angew. Chem., Int. Ed.* **2014**, *53*, 13720. (d) Freire, F.; Seco, J. M.; Quiñoá, E.; Riguera, R. *J. Am. Chem. Soc.* **2012**, *134*, 19374.
(15) (a) Kishimoto, Y.; Eckerle, P.; Miyatake, T.; Ikariya, T.; Noyori, R. *J. Am. Chem. Soc.* **1994**, *116*, 12131. (b) Tabata, M.; Yang, W.; Yokota, K. *Polym. J.* **1990**, *22*, 1105. (c) Furlani, A.; Napoletano, C.; Russo, M. V.; Feast, W. *Polym. Bull.* **1986**, *16*, 311. (d) Simionescu, C. I.; Percec, V. *J. Polym. Sci., Polym. Chem. Ed.* **1980**, *18*, 147. (e) Simionescu, C. I.; Percec, V. *J. Polym. Sci., Polym. Lett. Ed.* **1979**, *17*, 421. (f) Simionescu, C. I.; Percec, V.; Dumitrescu, S. *J. Polym. Sci., Polym. Chem. Ed.* **1977**, *15*, 2497.
(16) (a) Cheuk, K. K. L.; Li, B. S.; Lam, J. W. Y.; Tang, B. Z. *Macromolecules* **2008**, *41*, 5997. (b) Mayershofer, M. G.; Nuyken, O. *J. Polym. Sci., Part A: Polym. Chem.* **2005**, *43*, 5723. (c) Li, B. S.; Cheuk, K. K. L.; Ling, L.; Chen, J.; Xiao, X.; Bai, C.; Tang, B. Z. *Macromolecules* **2003**, *36*, 77. (d) Cheuk, K. K. L.; Lam, J. W. Y.; Chen, J.; Laiand, M. L.; Tang, B. Z. *Macromolecules* **2003**, *36*, 5947.
(17) Freire, F.; Seco, J. M.; Quiñoá, E.; Riguera, R. *Angew. Chem., Int. Ed.* **2011**, *50*, 11692.
(18) Louzao, I.; Seco, J. M.; Quiñoá, E.; Riguera, R. *Angew. Chem., Int. Ed.* **2010**, *49*, 1430.

DOI: 10.1021/jacs.6b04834
J. Am. Chem. Soc. 2016, 138, 9620−9628